Small molecule modulator of protein disulfide isomerase attenuates mutant huntingtin toxicity and inhibits endoplasmic reticulum stress in a mouse model of Huntington's disease

Xiao Zhou[#1], Gang Li[#1,2], Anna Kaplan[3], Michael M. Gaschler[4], Xiaoyan Zhang[1], Zhipeng Hou[5], Mali Jiang[1], Roseann Zott[6], Serge Cremers[6,7,8], Brent R. Stockwell[3,4], and Wenzhen Duan [1,9, 10*]

[1]Division of Neurobiology, Department of Psychiatry and Behavioral Sciences, Johns Hopkins University School of Medicine, Baltimore, MD 21287, USA. [2]Department of Pharmacology, Pharmacy School, Inner Mongolian Medical University, Hohhot, Inner Mongolian ,China; [3]Department of Biological Sciences, [4]Department of Chemistry, Columbia University, New York, NY 10027, USA; [5]Department of Radiology, Johns Hopkins University School of Medicine, Baltimore, MD 21287, USA; [6]Irving Institute for Clinical and Translational Research, [7]Department of Pathology and Cell Biology, [8]Department of Medicine, Columbia University Medical Center, New York, NY 10027, USA; [9]Program in Cellular and Molecular Medicine and [10]Department of Neuroscience, Johns Hopkins University School of Medicine, Baltimore, MD 21287, USA;

[#] These authors contributed to the work equally.

* Correspondence to: Wenzhen Duan, Division of Neurobiology, Department of Psychiatry and Behavioral Sciences, Johns Hopkins School of Medicine. CMSC 8-121, 600 North Wolfe Street, Baltimore, MD 21287. Tel: 410-502-2866; Fax: 410- 614-0013. Email: wduan2@jhmi.edu

Abstract

Huntington's disease (HD) is caused by a cytosine-adenine-guanine (CAG) trinucleotide repeat expansion in the huntingtin (HTT) gene encoding an elongated polyglutamine tract within the N-terminal of the Huntingtin protein (Htt) and leads to Htt misfolding, aberrant protein aggregation, and progressive appearance of disease symptoms. Chronic activation of endoplasmic reticulum (ER) stress by mutant Htt (mHtt) results in cellular dysfunction and ultimately cell death. Protein disulfide isomerase (PDI) is a chaperone protein located in the ER. Our previous studies demonstrated that mHtt caused PDI to accumulate at mitochondria-associated ER membranes and trigger cell death, and that modulating PDI activity using small molecules protected cells again mHtt toxicity in cell and brain slice models of HD. In this study, we demonstrated that the PDI is upregulated in the HD human brain, in cell and mouse models. Chronic administration of a reversible, brain penetrable small molecule PDI modulator, LOC14 (20 mg/kg/day), significantly improved motor function, attenuated brain atrophy, and extended survival in the N171-82Q HD mice. Moreover, LOC14 preserved medium spiny neuronal marker dopamine- and cyclic-AMP-regulated phosphoprotein of molecular weight 32,000 (DARPP32) levels in the striatum of HD mice. Mechanistic study revealed that LOC14 suppressed mHtt-induced ER stress, indicated by repressing the abnormally upregulated ER stress proteins in HD models. These findings suggest that LOC14 is promising to be further optimized for clinical trials of HD, and modulation of signaling pathways coping with ER stress may constitute an attractive approach to reduce mHtt toxicity and identify new therapeutic targets for treatment of HD.

Introduction

Huntington's disease (HD) is an inherited autosomal dominant neurodegenerative disorder characterized by degeneration and loss of neurons, particularly in the striatum. This genetic disorder is caused by the expansion of CAG repeats within the gene that encodes the poly-glutamine expanded huntingtin protein (Htt). Currently, no therapeutic avenue can delay the onset or prevent/slow the progression of the disease. There is an urgent need to develop therapeutics that can prevent or delay pathogenesis in HD. Although the mechanisms through which mutant Htt (mHtt) is deleterious to neuronal function remain elusive, accumulating data in HD models as well as human brain suggest that endoplasmic reticulum (ER) stress is implicated as an important contributor to mHtt toxicity in neurons (1). Evidence of induction of ER stress in human HD patients was provided in post-mortem HD patients' brain (2). Similarly, signs of ER stress were observed in HD mouse models at early stages of the disease (2, 3), and persists throughout the lifespan of these animals (2, 4, 5). It has been demonstrated that in striatal cells expressing full-length mHtt, expression of ER stress proteins, BiP, C/EBP homologous protein (CHOP) and protein disulfide isomerase (PDI), was increased compared with cells expressing normal Htt (5). These data suggest ER stress is linked to cell dysfunction/death in HD (6).

ER stress can be triggered by a number of conditions that interfere with oxidative protein-folding process, leading to the accumulation of abnormally folded proteins within ER (8). Mild ER stress engages the unfolded protein response (UPR) that increases the protein-folding capacity and quality control to reduce the unfolded protein load, or to trigger apoptosis to eliminate irreversibly damaged cells (9, 10). However, chronic and excessive ER stress can be detrimental and has been implicated as an important contributor to

polyglutamine toxicity in cells (6, 11, 12). Data from both yeast and mammalian cell models of HD have shown that ER stress and impaired ER-associated protein degradation (ERAD) are contributors to polyglutamine toxicity (5), for example, expression of mHtt N-terminal fragments upregulated UPR markers and increased cell death (13, 14), and inhibition of apoptosis signal-regulating kinase 1 protected HD mice by reducing ER stress (3).

PDI belongs to an ER chaperone family upregulated during ER stress that is responsible for the formation of disulfide bonds in proteins. PDI has two major functions. Firstly, it is responsible for the oxidation, reduction and isomerization of nonnative disulfide bonds in unfolded proteins entering the endoplasmic reticulum (ER). Secondly, PDI has general chaperone activity (15). Although PDI is generally associated with a protective effect in maintaining protein homeostasis, we and others showed that in certain circumstances, over activation of PDI is detrimental and trigger apoptosis (16, 17), distinct from its normal function in the UPR.

We previously reported that the pro-apoptotic function of PDI is specifically associated with expression of mHtt that resulted in accumulation of PDI at ER-mitochondrial junctions and apoptotic cell death, and that inhibition of PDI by small molecules prevented the neurotoxicity of mHtt *in vitro* (16). These data therefore point to a novel mechanism linking protein misfolding to apoptotic cell death induced by PDI in HD. It was shown that the amino terminal region of Htt interacts with the ER in a dynamic manner, forming an amphipathic α-helical membrane-binding domain that is affected under ER stress conditions, supporting the idea that Htt is an ER associated protein and the modulation of ER function could be beneficial in HD (1, 18, 19). In the present study, we report that LOC14, a previously identified reversible and noncovalent modulator of PDI which oxidizes the two cysteines in the active site of PDI and causes the

reduced thiols in PDI to become oxidized into a disulfide (**Supplemental Fig. 1**) (20), provided neuroprotective effects and suppressed ER stress in a mouse model of HD. Our results suggest that this class of reversible modulators of PDI may also have beneficial effects for other neurological disease caused by misfolded proteins and excessive ER stress.

Results

Mutant Htt upregulates PDI levels

In order to determine whether mHtt alters PDI levels in HD, we assessed the protein levels of two major PDI isoforms expressed in the brain, PDIA1 and PDIA3, by Western blotting analysis. Immortalized striatal cells expressing full-length mHtt (Q111) exhibited elevated levels of PDIA3 compared with cells expressing wild type Htt (Q7) (**Fig. 1A**). PDIA3 levels are also significantly upregulated in the striatum of mice expressing either N-terminal mHtt, N171-82Q HD (**Fig. 1B**), or a full-length mHtt (**Fig. 1C**), most importantly, increased PDIA3 levels were detected in the motor cortex (Brodmann area 4, BA4) of postmortem human HD brain (**Fig. 1D**). PDIA1 protein levels are slightly elevated in the striatal cells expressing mHtt, but not significantly altered in mouse or human HD brain (**Supplemental Fig. 2**). These results suggest that isoform-specific dysregulation of PDI occurs in HD.

The PDI modulator LOC14 improves motor function in N171-82Q HD mice

In light of our finding that PDI levels are upregulated in the striatum of N171-82Q HD mice, and our previous study indicated that inhibiting PDI protected cells against mHtt *in vitro* models (16, 20), and PDI modulator LOC14 protected cells from mHtt in brain slice model of HD (20), we set out goal to determine whether LOC14 has protective effects *in vivo*. We employed N171-82Q HD mouse model, because this

model is widely used to evaluate therapeutic efficacy, these HD mice exhibit progressive motor deficits, brain atrophy, body weight loss as well as shorter life span which recapitulate some of major symptoms manifested in HD patients.

We first confirmed the brain penetration and an appropriate dose of LOC14 for *in vivo* study. WT and HD mice were orally given (gavage) LOC14 at three different daily doses (10, 20, 50 mg/kg) for three days, blood (serum) and brain samples were collected for measurement of LOC14 concentrations three days after last drug administration. Our results indicated that LOC14 penetrated to mouse brain. Among three doses we tested, we selected medium dose 20 mg/kg/day for the chronic study based on the lower variability in drug concentrations in both brain and blood among animals administered with this dose (**Supplemental Fig. 3**). Pharmacokinetic parameters of LOC14 in mouse serum and brain following a single 20 mg/kg dose via IV Injection and Oral Gavage are shown in **Supplemental Table 1**. LOC14 at 50 mg/kg/day dose results in large variability in drug concentrations, particularly in the brain (striatum and cortex), indicating that drug absorption and/or brain distribution of LOC14 at this dose are not consistent.

We then examined whether oral administration of LOC14 could improve the motor function that is impaired in the N171-82Q HD mice. We employed balance beam (5 mm diameter) and a tapered beam to evaluate motor coordination. HD mice displayed prolonged transverse time on a 5 mm balance beam at ages of 24 weeks (genotype main effect, $F=12.58$, $t=4.205$, $p<0.001$) and 28 weeks (genotype main effect, $F=22.428$, $t=5.594$, $p<0.001$) compared to their age, gender-matched wild type mice (**Fig.2 A, C**), indicating motor deficits in the HD mice. Oral administration of LOC14 significantly improved the motor performance of HD mice on 5 mm beam, indicated by shortened transverse time on the beam at 24 weeks (treatment main effect within HD mice, $F=4.5$, $t=2.957$, $p=0.006$) and 28 weeks of age (treatment main

effect within HD mice, F=7.838, t=3.905, $p<0.001$) (**Fig. 2A, C**). Similarly, HD mice displayed prolonged transverse time on a tapered beam at ages of 24 weeks (genotype main effect, F=18.904, t=4.262, $p<0.001$) and 28 weeks (genotype main effect, F=25.018, t=5.282, $p<0.001$) compared to their age, gender-matched wild type mice (**Fig.2 B, D**). Oral administration of LOC14 significantly improved the motor performance of HD mice on a tapered beam, indicated by shortened transverse time on the beam at 24 weeks (treatment main effect within HD mice, F=2.969, t=2.231, $p=0.032$) and 28 weeks of age (treatment main effect within HD mice, F=1.619, t=2.3435, $p<0.026$) (**Fig. 2B, D**). These results indicated that LOC14 administration significantly improved motor function in HD mice.

The PDI modulator LOC14 attenuates brain atrophy in N171-82Q HD mice

To determine whether improved motor function in HD mice treated with LOC14 resulted from slowed progression of the neurodegenerative process and/or prevention of pathogenesis in the brain, we used *in vivo* structural MRI scans to measure brain volumes after 14 weeks of LOC14 administration (at the age of 26 weeks). As we demonstrated previously, as the disease progressed, N171-82Q HD mice displayed significant regional and whole brain atrophy (21).

N171-82Q HD mice exhibited significant atrophy in the striatum (about 18% volume loss, t=6.627, $p<0.001$), neocortex (19% volume loss, t=9.302, $p<0.001$), as well as whole brain volume loss (19% reduction, t=7.374, $p<0.001$) at the age of 26 weeks compared to the age- and gender- matched wild type mice. Oral administration of LOC14 significantly attenuated the magnitude of atrophy in the striatum (61% rescue by LOC14, t=2.485, $p=0.027$) (**Fig 3A-B**), neocortex (26 % rescue by LOC14, t=2.717, $p=0.018$) (**Fig. 3C**,), as well as whole brain (47% rescue by LOC14, t=3.882, p=0.004) (**Fig. 3D)**. The brain atrophy in N171-82Q HD mice display region-specific vulnerability pattern similar to that in human

HD, we did not observe significant atrophy in the cerebellum of N171-82Q HD mice and LOC14 had no effects on cerebellum volume (p=0.431) (**Fig. 3E**).

The PDI modulator LOC14 preserves DARPP32 levels and improves survival in N171-82Q HD mice

DARPP32 is a fundamental component of the dopamine-signaling cascade, and HD pathology is marked by extensive loss of medium spiny neurons in the striatum that express high levels of DARPP32; therefore, DARPP32 serves as a marker of neuronal dysfunction or neuronal loss in HD (22, 23). We observed significantly reduced DARPP-32 levels in the striatum of N171-82Q HD mice (genotype main effect, F=75.45, t=14.61, p<0.001), as we reported previously (24), and the decreased DARPP32 levels were restored by oral administration of LOC14 (treatment main effect, F=63.32, t=14.10, p<0.001) (**Fig. 4A**), suggesting that LOC14 protected medium spiny neurons from degeneration or dysfunction.

It is noteworthy that most HD mouse models, including N171-82Q, show significant brain atrophy, but not striking neuronal death. The loss of DARPP32 levels possibly result from neuronal dysfunction instead of neuronal death in this model. LOC14 prevented loss of DARPP32, and preserved the function of medium spiny neurons in the striatum, though LOC14 did not completely prevent striatal atrophy.

In addition to neurological features, N171-82Q HD mice also display metabolic abnormalities, including body waste that is observed in several HD mouse models as well as in HD patients. We then determined whether LOC14 has effect on body weight. Our results indicated that LOC14 at 20mg/kg/day, the dose used in the efficacy study, had no significant effects on body weight loss in HD mice throughout the treatment periods (**Supplemental Fig. 4**).

In addition, N171-82Q HD mice exhibit shorter life span. LOC14 extended the survival of N171-82Q mice modestly but significantly (4.4% increase, 226 ± 7 in HD -Vehicle group and 236 ± 2 in HD-LOC14 group; p=0.039. Kaplan-Meier survival analysis) (**Fig. 4B**). It is not known why HD mice die. Notably, HD patients often die from complications of pneumonia. It can therefore be argued that survival as an outcome measure in HD-like mice, although sometimes useful, does not always directly inform us about neurological progression. Metabolic abnormalities may contribute to the death of N171-82Q HD mice, we found that LOC14 did not alter the body weight loss in HD mice (**Supplemental Fig. 4**), which might explain why LOC14 dramatically improved motor function and attenuated brain atrophy, but the extended the survival is modest.

The PDI modulator LOC14 suppresses ER stress in N171-82Q HD mouse brain.

It is suggested a direct correlation between disease progression and the occurrence of ER stress in HD models (1). Increased expression of downstream UPR effectors, such as the X-box binding protein 1 (XBP1), BiP/GRP78, CHOP was reported in human post-mortem HD brain (2). To determine whether ER stress involved in the protective mechanism of LOC14 in N171-82Q HD mice, we measured ER stress protein levels in mouse brain. We observed that levels of ER stress responsive proteins, including XBP1 (genotype effect, F=36.28, t=7.91, p<0.001), CHOP (genotype effect, F=21.53, t=5.96, p<0.001) and Bip (genotype effect, F=11.37, t=4.31, p=0.003), were significantly upregulated in N171-82Q HD mouse brain compared those in age-, gender-matched wild type mice. LOC14 (20 mg/kg/day) oral administration significantly suppressed these ER stress protein levels, including XBP1 (treatment effect, F=29.18, t=7.46, p<0.001) (**Fig. 5B**), CHOP (treatment effect, F= 2.093, t=3.707, p=0.006) (**Fig. 5C**), and Bip (treatment

effect, F=2.958, t=3.145, p=0.014) (**Fig 5D**) in HD mice, suggesting that LOC14 reduces excessive ER stress in N171-82Q HD mice.

The PDI modulator LOC14 protects cells from mHtt by reducing ER stress

To examine direct effect of LOC14 on ER stress response, we employed mouse striatal cell model expressing either full-length wild-type (STHdhQ7/7) or mutant (STHdhQ111/111) Htt under the endogenous promoter and expressing at endogenous levels (25). The mHtt-induced dysfunction is detected by reduction of ATP levels in these cells (25). We confirmed that the striatal cells expressing mHtt exhibited reduced ATP levels at 24 h after serum withdrawal; cells treated with LOC14 significantly preserved ATP levels at a concentration-dependent manner from 5 nM to 40 nM (**Fig. 6A**), indicating a direct cell protective effect of LOC14 against mHtt.

mHtt expressing striatal cells also exhibited enhanced ER stress in response to serum deprivation, indicated by upregulation of CHOP (genotype effect, F=7.062, t=4.215, p=0.003) (**Fig. 6 B&C**), Bip (genotype effect, F=5.413, t=3.453, p=0.009) (**Fig. 6 B&D**), and PDIA3 levels (genotype effect, F=7.288, t=3.385, p=0.01) (**Fig. 6B&E**). Interestingly, LOC14 not only inhibited the upregulation of these ER stress response proteins CHOP (treatment effect, F=29.18, t=7.46, p<0.001) (**Fig. 6C**) and Bip (treatment effect, F=1.178, t=2.575, p=0.033) (**Fig. 6D***)*, but also brought the PDIA3 levels to the normal range (treatment effect, F=7.351, t=3.393, p=0.009) (**Fig. 6E**).

Discussion

In the last decade, the traditional view of ER and mitochondria as two independent organelles has been profoundly challenged. Presently, it is known that ER and mitochondria are physically interconnected in a

zone called mitochondria-associated membranes (MAM) (26, 27). Neurons critically depend on mitochondria-associated membranes as a means to exchange metabolites and signaling molecules between these organelles (28, 29). It is believed that the communication between ER and mitochondria is essential to the maintenance of mitochondrial dynamics and cell function (30). In ER, an overload of misfolded mHtt may cause ER stress and upregulation of PDI, which assists refolding at the beginning stage of ER response to stress. However, as prolonged ER stress, elevated PDI is coupled with increased activity of ER oxidoreductin 1 (Ero1), producing harmful hydroperoxide, excessive activation of PDI-Ero1 cycle by an increased influx of mHtt may cause overproduction of hydrogen peroxide and promote additional reactive oxygen species generation and oxidative stress to cells. We have shown previously that mHtt caused PDI to accumulate at MAM and triggered cell death via increased mitochondrial outer-membrane permeabilization (16). Furthermore, in brain-slice assays for neurodegeneration induced by mHtt, PDI modulator LOC14 had neuroprotective effects (20). The present study validated that inhibition of PDI enzymatic activity rescued mHtt-induced motor dysfunction and brain pathology *in vivo* mouse model of HD.

The presence of mHtt does not acutely or even necessarily directly kill cells. Instead, mHtt expression increases cell susceptibility to various stresses, such as aging and oxidative stress. Misfolded mHtt protein could accumulate and activate ER stress. The mechanism of increased sensitivity to ER stress in mHtt expressing cells appears to be a complex. A likely underlying mechanism came with the finding that mHtt expression decreased rates of turnover of an ER associated degradation substrate; this is in line with previous reports that mHtt-expressing cells had decreased activity of the ubiquitin-proteasome system (31-33). The inability of cells to cope with ER stress could represent an important modulator of the mHtt toxicity. Silencing XBP-1 expression in the full-length mHtt expressing mice reduces neuronal loss in the

striatum and improves motor performance (34), indicating that suppressing ER stress can modulate mHtt neurotoxicity. Our current results from both mouse brain and cell model suggest that LOC14 could suppress upregulated XBP-1 induced by mHtt, thereby protecting cells from mHtt-induced ER stress. ER stress protein CHOP is a transcription factor, after its activation, CHOP upregulates the Ero1α leading to an excessive generation of oxidants, depletion of the antioxidant glutathione (35). The upregulation of CHOP can also downregulate Bcl2 and upregulate pro-apoptotic Bax and Bak (36-38). LOC14 suppressed CHOP upregulation induced by mHtt, therefore reduced the consequent oxidative stress insults and pro-apoptotic effects of CHOP.

In our previous study, we identified and characterized LOC14 as the first reversible, neuroprotective, nanomolar modulator of PDI. We found that LOC14 reversibly binds to a region adjacent to the active site of PDI, induces the protein to adopt an oxidized conformation, and inhibits its reductase activity, and the oxidation of PDI by LOC14 is protective in PC12 cells and in medium spiny neurons that degenerate from mHtt expression (20). The present study is the first report that modulation of PDI activity by LOC14 exhibited neuroprotective effects *in vivo*, indicated by significantly improved motor function, attenuated brain atrophy and preserved DARPP32 levels in HD mice. LOC14 penetrates the blood-brain barrier well and reached the effective concentrations in the brain. The current findings provide validation for LOC14 as a promising candidate to be considered in HD clinical trials.

Materials and Methods

Mice, human brain samples, LOC14 synthesis and administration

Male N171-82Q HD mice were mated to female hybrid mice (B6C3F1/J, Jackson Laboratory, ME). Male mice were used in our studies because gender-dependent phenotypic differences in N171-82Q HD mice were identified previously. Mice were randomly divided into four groups. All mice were used in analyses. Postmortem brain samples were provided by the Johns Hopkins Neuropathology Brain Bank. The samples are from Brodmann area 4 (BA4) (motor cortex) region. The stage of HD ranges from Vonsattel Grade 3 and Grade 4. Samples are from male, white Caucasian in both control and HD group. Ages are 70 ± 5 years. CAG size ranges from 42 to 45. The post-mortem intervals were approximately 16-20 h.

2-((4-(cyclopropanecarbonyl)piperazin-1-yl)methyl)benzo[d]isothiazol3(2H)-one (LOC14) was synthesized in our laboratory and its structure was shown previously (20). Briefly, all commercial reagents were used without further purification. All solvents used were reagent or HPLC grade. All reactions were carried out in flame-dried glassware under a nitrogen atmosphere. Chemical yields refer to isolated, spectroscopically pure compounds. 1H and 13C NMR spectra were recorded on a 400 or 500 MHz spectrometer at ambient temperature. Chemical shifts are recorded in parts per million relative to residual solvent CDCl3 (1H, 7.26 ppm; 13C, 77.16 ppm). Multiplicities are reported as follows: s = singlet, d = doublet, t = triplet, bs = broad singlet, m = multiplet, comp m = complex multiplet, td = triplet of doublets, dt = doublet of triplets, ddd = doublet of doublet of doublets. In an open round bottom flask, methanol (20 mL) and a 38% solution of formaldehyde in water (4.1 mL 1.2 eq.) were combined. 1,2-Benzisothiazol-3(2H)-one (5.2 g, 1 eq.). The suspension was stirred at 30 ºC until all solids were dissolved. 1-(cyclopropylcarbonyl)piperazine (4.87 mL, 1 eq.) was added and the heat was removed, allowing the solution to return to room temperature. With cooling, solids precipitated out of solution. These solids were collected via filtration and washed with hexanes. The solids were dissolved in a minimum of ethyl acetate and recrystallized by slow addition of hexanes, providing LOC14 (7.2g, 66%) as

a white crystalline mass. 1H NMR (400 MHz, Chloroform-d) δ 8.03 (dt, J = 7.9, 1.0 Hz, 1H), 7.63 (t, J = 7.1, 1H), 7.55 (d, J = 8.1, 1H), 7.41 (ddd, J = 8.0, 7.1, 1.0 Hz, 1H), 4.74 (s, 2H), 3.68 (bs, 4H), 2.78 – 2.69 (bs, 4H), 1.69 (m, 1H), 0.99 – 0.91 (m, 2H), 0.80 – 0.67 (m, 2H). 13C NMR (500 MHz, CDCl3) δ 172.1, 166.7, 141.1, 132.2, 126.8, 125.7, 124.7, 120.4, 65.0, 50.7, 50.9, 45.4, 42.0, 11.2, 7.5.

LOC14 was freshly prepared by first dissolving in 1-Methyl-2-pyrrolidinone (NMP, Sigma Cat# 328634) to make 80 mg/ml stock solution and then diluted by 0.5% methyl cellulose to the final concentration (40 × dilution). LOC14 or vehicle was orally administered to the mice by gavage from 12 weeks old age to the end of study. All animal experiments were performed according to procedures approved by the Institutional Animal Care and Use Committee of the Johns Hopkins University and following guideline of National Institute of Health.

Measurement of LOC14 levels by LC-MS/MS in mouse brain and serum

LOC14 levels were measured in mouse plasma, striatum, and cerebral cortex using Ultra Performance Liquid Chromatography-Tandem Mass Spectrometry (LC-MS/MS). LOC14 was extracted from mouse plasma by mixing 100 µl of plasma with 900 µl of cold acetonitrile containing 25 ng/ml of cyclocreatine as an internal standard. After mixing for 5 min. the sample was centrifuged for 10min and the organic layer was transferred to an LC-MS vial and dried under nitrogen. The sample was reconstituted in 100 µl of 50% acetonitrile and 5 µl was injected onto the LC-MS. Brain tissue samples were homogenized using a tissue tearor at a concentration of 150 mg/ml in cold LC-MS water followed by extraction with 1.8 ml of cold acetonitrile containing the cyclocreatine internal standard. The brain samples were mixed and centrifuged and reconstituted the same as for the plasma samples. Calibration standards were also prepared spanning a range of 1 ng/ml to 100 ng/ml and extracted in the same manner as the samples.

LC-MS/MS analysis was performed on a platform comprising a triple quadrupole Waters Xevo TQ-S (Waters, Milford, MA) equipped with an electrospray ionization source and integrated with a Waters Acquity UHPLC controlled by Mass Lynx Software 4.1. Chromatographic separation was performed utilizing a Waters UPLC HSS T3 column (2.1 x 100mm) maintained at 50°C. The flow rate was maintained at 400 µl /min. The initial flow conditions were 90% solvent A (water containing .01% acetic acid) and 10% solvent B (methanol containing 0.1% acetic acid). Solvent B was raised to 50% over 3 min and to 98% by 4 min, lowered to 50% by 6 min and back to initial conditions by 7 min with a total run time of 7.5 min. The mass spectrometer was operated under multiple reaction monitoring (MRM) mode with positive electrospray ionization with the following parameters: Capillary voltage: 1.3Kv, Cone gas flow: 150 L/h; desolvation gas: 1000 L/h; and gas temperature: 500 °C. The transition 155.10 > 87.11 was utilized for quantitation. Peak integration and data analysis were performed with Target Lynx 4.1. The intra-assay precision for the assay was 6.00%.

Balance beam tests and survival

Motor function was assessed on an 80-cm long and 5-mm wide square-shaped balance beam that was mounted on supports 50-cm in height. A bright light illuminated the start platform, and a darkened enclosed 1728 cm^3 escape box (12 × 12 × 12 cm) was situated at the end of the beam. Disposable pads placed under the beam provided cushioning if an animal fell off the beam. Mice were trained to walk across the beam twice at least 1 h prior to testing. If a mouse stopped during training, the tail was gently pressed to encourage movement. After the training trial, mice were left undisturbed for at least an hour before testing. The time for each mouse to traverse the balance beam was recorded with a 60 s maximum cut-off, and falls were scored as 60 s. In addition to the 5 mm balance beam, the tapered beam was also

used to evaluate hindlimb function. To increase sensitivity of the task and to encourage the mice to run the beam reliably, the beam was angled at 17° from the horizontal such that the mouse was able to run uphill. Our apparatus also has a goal box, as the use of a goal box can be beneficial for expediting training and increasing the reliability of the test performance. As the beam is elevated above ground level, a soft landing area is essential beneath the beam, which in our laboratory consists of numerous bench pads. The traverse time when the mouse crossed the start line and ended was recorded.

Survival was monitored daily by an experienced investigator (G.L). The mice were considered at the end of life when they were unable to right themselves after being placed on their backs and initiate movement after being gently prodded for 30 sec.

In vivo structural MRI acquisition and quantification

In vivo structural MRI scans were performed on a horizontal 9.4T magnetic resonance imager (Bruker Biospin, Billerica) with a triple axis gradient and an animal imaging probe. The detailed image capture and analysis were described in our previous study (Cheng et al., 2011). Briefly, mice were anesthetized with 1% isoflurane, respiration was monitored and the temperature was maintained during the entire scan. Images were acquired by a three-dimensional T2-weighted fast spin echo sequence with the following parameters: echo time (TE)/repetition time (TR) = 40/700 ms, resolution = 0.1 mm × 0.1 mm × 0.1 mm, echo train length = 4, number of average = 2 and flip angle =40°. The imaging resolution and contrast were sufficient for automatic volumetric characterization of the mouse brains and substructures. The intensity-normalized images were submitted by the Diffeomap software to a linux cluster, which runs Large Deformation Diffeomorphic Metric Mapping (LDDMM). The transformations encode

morphological differences between subject and template images and can be analyzed with deformation-based morphometry to detect regional changes in brain volume.

Protein extraction and Western blot analysis

Striatal tissue samples were homogenized in a buffer containing 50 mM Tris-HCl, pH 8.0, 150 mM NaCl, 0.1% (w/v) SDS, 1.0% NP-40, 0.5% sodium deoxycholate, and 1% (v/v) freshly prepared protease inhibitor mixture. For SDS PAGE, 10–20 μg of proteins were separated in a 4-20% gradient gel and transferred to a nitrocellulose membrane. The membrane was blotted with the following primary antibodies: anti-PDIA1 (Sigma, 1:1000), anti-PDIA3 (Sigma, 1:500), anti-XBP1 (Sigma, 1:1000), anti-DARPP32 (Abcam, 1:1000), anti-CHOP (Sigma, 1:1000), anti-Bip (Cell Signaling, 1:1000), and mouse anti-β-actin (Sigma, 1:5000). After incubation with HRP-conjugated secondary antibodies, the bound antibodies were visualized by chemiluminescence. The intensity of the Western blot bands was quantified by Image J software.

Measurement of ATP levels

Cell viability was measured by the CellTiter-Glo® Luminescent Cell Viability Assay, in which the amount of ATP was quantified by luminescence signal. Briefly, cells were cultured in opaque-walled 96-well plates with the same density at 10,000/100 μl per well. After the indicated treatment, the plate and its contents were equilibrated at room temperature for about 30 min and 100 μl of CellTiter-Glo® reagent (Promega) were added to each well and mixed thoroughly. The plate was then maintained at room temperature for 10 min. Luminescence signal was measured with a FluoroSkan Acsent FL luminescence reader (Thermo Lab system).

Statistics

Data are expressed as the mean ± SEM unless otherwise noted. Statistical analyses were performed using Student's *t*-tests between two groups (Fig. 1), one-way *ANOVA and Holm-Sidak* tests among multiple groups with one factor involved between two comparing groups (Fig. 3), or two-way *ANOVA* and Bonferroni *post hoc* tests among multiple groups when there are two factors involved in comparing groups (Figs. 2, 4, 5, 6) (significance markers on figures) unless otherwise noted. Survival data were analyzed by Kaplan-Meier analysis. Differences were considered statistically significant for $p < 0.05$. N is reported in the figure legends.

Acknowledgments

We thank Mr. Hao Gu and Ms Qi Peng for technical assistance with animal colony maintenance, drug administration and animal tissue collection; Drs. Juan Troncoso and Olga Pletinikova at the Johns Hopkins Neuropathology for providing the human postmortem brain samples. The research was supported by NIH grants R01NS082338, R21NS094886, R21NS099670 (to W.D.) and funding from the Alzheimer's Drug Discovery Foundation (to B.R.S.).

Conflict of Interest statement. None declared.

References

1 Vidal, R., Caballero, B., Couve, A. and Hetz, C. (2011) Converging pathways in the occurrence of endoplasmic reticulum (ER) stress in Huntington's diSEaSE. *Curr. Mol .Med.*, **11**, 1-12.

2 Carnemolla, A., Fossale, E., Agostoni, E., Michelazzi, S., Calligaris, R., De Maso, L., Del Sal, G., MacDonald, M.E. and Persichetti, F. (2009) Rrs1 is involved in endoplasmic reticulum stress responSE in Huntington diSEaSE. *J. Biol. Chem.*, **284**, 18167-18173.

3 Cho, K.J., Lee, B.I., Cheon, S.Y., Kim, H.W., Kim, H.J. and Kim, G.W. (2009) Inhibition of apoptosis signal-regulating kinaSE 1 reduces endoplasmic reticulum stress and nuclear huntingtin fragments in a mouSE model of Huntington diSEaSE. *Neuroscience*, **163**, 1128-1134.

4 Garcia-Martinez, J.M., Perez-Navarro, E., Xifro, X., Canals, J.M., Diaz-Hernandez, M., Trioulier, Y., Brouillet, E., Lucas, J.J. and Alberch, J. (2007) BH3-only proteins Bid and Bim(EL) are differentially involved in neuronal dysfunction in mouSE models of Huntington's diSEaSE. *J. Neurosci. Res.*, **85**, 2756-2769.

5 Duennwald, M.L. and Lindquist, S. (2008) Impaired ERAD and ER stress are early and specific events in polyglutamine toxicity. *Genes Dev.*, **22**, 3308-3319.

6 Kouroku, Y., Fujita, E., Jimbo, A., Kikuchi, T., Yamagata, T., Momoi, M.Y., Kominami, E., Kuida, K., Sakamaki, K., Yonehara, S. *et al.* (2002) Polyglutamine aggregates stimulate ER stress signals and caspaSE-12 activation. *Hum. Mol. Genet.*, **11**, 1505-1515.

7 Higo, T., Hamada, K., Hisatsune, C., Nukina, N., Hashikawa, T., Hattori, M., Nakamura, T. and Mikoshiba, K. (2010) Mechanism of ER stress-induced brain damage by IP(3) receptor. *Neuron*, **68**, 865-878.

8 Ron, D. and Walter, P. (2007) Signal integration in the endoplasmic reticulum unfolded protein responSE. *Nat. Rev. Mol. Cell. Biol.*, **8**, 519-529.

9 Woehlbier, U. and Hetz, C. (2011) Modulating stress responSEs by the UPRosome: a matter of life and death. *Trends Biochem. Sci.*, **36**, 329-337.

10 Hetz, C. (2012) The unfolded protein responSE: controlling cell fate decisions under ER stress and beyond. *Nat. Rev. Mol. Cell. Biol.*, **13**, 89-102.

11 Nishitoh, H., Matsuzawa, A., Tobiume, K., Saegusa, K., Takeda, K., Inoue, K., Hori, S., Kakizuka, A. and Ichijo, H. (2002) ASK1 is esSEntial for endoplasmic reticulum stress-induced neuronal cell death triggered by expanded polyglutamine repeats. *Genes Dev.*, **16**, 1345-1355.

12 Thomas, M., Yu, Z., Dadgar, N., Varambally, S., Yu, J., Chinnaiyan, A.M. and Lieberman, A.P. (2005) The unfolded protein responSE modulates toxicity of the expanded glutamine androgen receptor. *J. Biol. Chem.*, **280**, 21264-21271.

13 Reijonen, S., Putkonen, N., Norremolle, A., Lindholm, D. and Korhonen, L. (2008) Inhibition of endoplasmic reticulum stress counteracts neuronal cell death and protein aggregation cauSEd by N-terminal mutant huntingtin proteins. *Exp. Cell. Res.*, **314**, 950-960.

14 Safren, N., El Ayadi, A., Chang, L., Terrillion, C.E., Gould, T.D., Boehning, D.F. and Monteiro, M.J. (2014) Ubiquilin-1 overexpression increaSEs the lifespan and delays accumulation of Huntingtin aggregates in the R6/2 mouSE model of Huntington's diSEaSE.

PLoS One, **9**, e87513.

15 Ferrari, D.M. and Soling, H.D. (1999) The protein disulphide-isomeraSE family: unravelling a string of folds. *Biochem. J.*, **339 (Pt 1)**, 1-10.

16 Hoffstrom, B.G., Kaplan, A., Letso, R., Schmid, R.S., Turmel, G.J., Lo, D.C. and Stockwell, B.R. (2010) Inhibitors of protein disulfide isomeraSE suppress apoptosis induced by misfolded proteins. *Nat. Chem. Biol.*, **6**, 900-906.

17 Zhao, G., Lu, H. and Li, C. (2015) Proapoptotic activities of protein disulfide isomeraSE (PDI) and PDIA3 protein, a role of the Bcl-2 protein Bak. *J. Biol. Chem.*, **290**, 8949-8963.

18 Atwal, R.S. and Truant, R. (2008) A stress SEnsitive ER membrane-association domain in Huntingtin protein defines a potential role for Huntingtin in the regulation of autophagy. *Autophagy*, **4**, 91-93.

19 Atwal, R.S., Xia, J., Pinchev, D., Taylor, J., Epand, R.M. and Truant, R. (2007) Huntingtin has a membrane association signal that can modulate huntingtin aggregation, nuclear entry and toxicity. *Hum. Mol. Genet.*, **16**, 2600-2615.

20 Kaplan, A., Gaschler, M.M., Dunn, D.E., Colligan, R., Brown, L.M., Palmer, A.G., 3rd, Lo, D.C. and Stockwell, B.R. (2015) Small molecule-induced oxidation of protein disulfide isomeraSE is neuroprotective. *Proc. Natl. Acad. Sci. U S A*, **112**, E2245-2252.

21 Cheng, Y., Peng, Q., Hou, Z., Aggarwal, M., Zhang, J., Mori, S., Ross, C.A. and Duan, W. (2011) Structural MRI detects progressive regional brain atrophy and neuroprotective effects in N171-82Q Huntington's diSEaSE mouSE model. *Neuroimage*, **56**, 1027-1034.

22 Vonsattel, J.P., Myers, R.H., Stevens, T.J., Ferrante, R.J., Bird, E.D. and Richardson, E.P., Jr. (1985) Neuropathological classification of Huntington's diSEaSE. *J. Neuropathol. Exp.*

Neurol., **44**, 559-577.

23 de la Monte, S.M., Vonsattel, J.P. and Richardson, E.P., Jr. (1988) Morphometric demonstration of atrophic changes in the cerebral cortex, white matter, and neostriatum in Huntington's diSEaSE. *J Neuropathol Exp. Neurol.*, **47**, 516-525.

24 Jiang, M., Wang, J., Fu, J., Du, L., Jeong, H., West, T., Xiang, L., Peng, Q., Hou, Z., Cai, H. *et al.* (2012) Neuroprotective role of Sirt1 in mammalian models of Huntington's diSEaSE through activation of multiple Sirt1 targets. *Nat. Med.*, **18**, 153-158.

25 Trettel, F., Rigamonti, D., Hilditch-Maguire, P., Wheeler, V.C., Sharp, A.H., Persichetti, F., Cattaneo, E. and MacDonald, M.E. (2000) Dominant phenotypes produced by the HD mutation in STHdh(Q111) striatal cells. *Hum. Mol. Genet.*, **9**, 2799-2809.

26 Kornmann, B. (2013) The molecular hug between the ER and the mitochondria. *Curr. Opin. Cell Biol.*, **25**, 443-448.

27 van Vliet, A.R., Verfaillie, T. and Agostinis, P. (2014) New functions of mitochondria associated membranes in cellular signaling. *Biochim. Biophys. Acta*, **1843**, 2253-2262.

28 Szymanski, J., Janikiewicz, J., Michalska, B., Patalas-Krawczyk, P., Perrone, M., Ziolkowski, W., Duszynski, J., Pinton, P., Dobrzyn, A. and Wieckowski, M.R. (2017) Interaction of Mitochondria with the Endoplasmic Reticulum and Plasma Membrane in Calcium Homeostasis, Lipid Trafficking and Mitochondrial Structure. *Int. J. Mol. Sci.*, **18**.

29 Krols, M., van Isterdael, G., AsSElbergh, B., Kremer, A., Lippens, S., Timmerman, V. and JansSEns, S. (2016) Mitochondria-associated membranes as hubs for neurodegeneration. *Acta Neuropathol.*, **131**, 505-523.

30 Friedman, J.R., Lackner, L.L., West, M., DiBenedetto, J.R., Nunnari, J. and Voeltz, G.K.

(2011) ER tubules mark sites of mitochondrial division. *Science*, **334**, 358-362.

31 Bennett, E.J., Shaler, T.A., Woodman, B., Ryu, K.Y., ZaitSEva, T.S., Becker, C.H., Bates, G.P., Schulman, H. and Kopito, R.R. (2007) Global changes to the ubiquitin system in Huntington's diSEaSE. *Nature*, **448**, 704-708.

32 Godin, J.D., Poizat, G., Hickey, M.A., Maschat, F. and Humbert, S. (2010) Mutant huntingtin-impaired degradation of beta-catenin cauSEs neurotoxicity in Huntington's diSEaSE. *EMBO J.*, **29**, 2433-2445.

33 Tydlacka, S., Wang, C.E., Wang, X., Li, S. and Li, X.J. (2008) Differential activities of the ubiquitin-proteasome system in neurons versus glia may account for the preferential accumulation of misfolded proteins in neurons. *J. Neurosci.*, **28**, 13285-13295.

34 Vidal, R.L., Figueroa, A., Court, F.A., Thielen, P., Molina, C., Wirth, C., Caballero, B., Kiffin, R., SEgura-Aguilar, J., Cuervo, A.M. *et al.* (2012) Targeting the UPR transcription factor XBP1 protects against Huntington's diSEaSE through the regulation of FoxO1 and autophagy. *Hum. Mol. Genet.*, **21**, 2245-2262.

35 Oyadomari, S. and Mori, M. (2004) Roles of CHOP/GADD153 in endoplasmic reticulum stress. *Cell Death Differ.*, **11**, 381-389.

36 Li, G., Mongillo, M., Chin, K.T., Harding, H., Ron, D., Marks, A.R. and Tabas, I. (2009) Role of ERO1-alpha-mediated stimulation of inositol 1,4,5-triphosphate receptor activity in endoplasmic reticulum stress-induced apoptosis. *J. Cell Biol.*, **186**, 783-792.

37 Han, J., Back, S.H., Hur, J., Lin, Y.H., Gildersleeve, R., Shan, J., Yuan, C.L., Krokowski, D., Wang, S., Hatzoglou, M. *et al.* (2013) ER-stress-induced transcriptional regulation increaSEs protein synthesis leading to cell death. *Nat. Cell Biol.*, **15**, 481-490.

38 Logue, S.E., Cleary, P., Saveljeva, S. and Samali, A. (2013) New directions in ER stress-induced cell death. *Apoptosis*, **18**, 537-546.

Legends to Figures

Figure 1. PDIA3 levels are increased in Huntington's disease (HD). (**A**) Immortalized striatal cells expressing full-length huntingtin with either wild type form (Q7) or mutant form (Q111). Cell lysates were collected and PDIA3 protein levels were assessed. (**B**) Mouse striatal samples were collected from N171-82Q HD transgenic mice and their littermate wild type (WT) mice, the PDIA3 levels were assessed by Western blotting. N=5. (**C**) Mouse striatal samples were collected from 6 month-old zQ175full-length huntingtin knock-in mice and their littermate control mice. N=4. (**D**) Postmortem human brain tissue (BA4 cortex) was collected and PDIA3 levels were assessed. N=4. *$p<0.05$ compared with the WT or control group by Standard Student's *t*-tests.

Figure 2. 2-((4-(cyclopropanecarbonyl)piperazin-1-yl)methyl)benzo[d]isothiazol3(2H)-one (LOC14) rescues motor deficits in N171-82Q HD mice. LOC14 (20 mg/kg/day) was orally administered to mice daily from 12 weeks of age. Mice were tested on a 5-mm square-shaped beam or a tapered beam at 24 (**A &B**) and 28 (**C& D**) weeks of age. N=10-13 mice. The values are the mean ± SEM, *$p<0.05$ compared with the values of wild type (WT)-vehicle group; **$p<0.05$ compared with the value of HD-vehicle group by two-way *ANOVA* and Bonferroni *post hoc* tests.

Figure 3. 2-((4-(cyclopropanecarbonyl)piperazin-1-yl)methyl)benzo[d]isothiazol3(2H)-one (LOC14) attenuated brain atrophy in N171-82Q HD mice. LOC14 (20 mg/kg/day) was orally administered to mice daily from 12 weeks of age, and *in vivo* structural MRI were obtained at 26 weeks of age. Brain volumes were calculated by Large Deformation Diffeomorphic Metric Mapping (LDDMM). (**A**) Representative MRI images. Scale bars 60 μm. CX is for neocortex and S for striatum. (**B-E**) Quantification of regional

brain volumes by structural MRI as indicated in each graph. Values are mean ± SEM from five mice in each group. * $p<0.05$ compared with the WT- vehicle value; ** $p<0.05$ compared with the HD-vehicle value, one-way *ANOVA and Holm-Sidak* test.

Figure 4. 2-((4-(cyclopropanecarbonyl)piperazin-1-yl)methyl)benzo[d]isothiazol3(2H)-one (LOC14) preserves DARPP32 levels in the striatum and extended survival of N171-82Q HD mice. (**A**) LOC14 (20mg/kg) was administered to mice daily from 12 weeks of age; (**A**) Mice were euthanized at 24 weeks of age and the striatum was dissected for measurement of DARPP32 levels by Western blotting. Top, representative blots and bottom, densitometry results from three mice in each group. All values are mean ± SEM. N=3. * $p<0.05$, compared to the value of WT vehicle group; **p<0.05 compared to the value of HD-vehicle group. Two-way *ANOVA* and Bonferroni *post hoc* tests. (**B**) Survival was monitored daily, mice were considered to be at the end of life when they were unable to right themselves after being placed on their backs and initiate movement after being gently prodded for 30 sec. * $p<0.05$ between HD-vehicle (N=10) and HD-LOC14 (N=12) groups by log rank analysis.

Figure 5. 2-((4-(cyclopropanecarbonyl)piperazin-1-yl)methyl)benzo[d]isothiazol3(2H)-one (LOC14) suppressed mutant Htt-induced endoplasmic reticulum (ER) stress. (**A**) Representative Western blots with indicated ER stress responsive proteins. (**B-D**) Quantification of protein levels of each ER stress protein in the striatum from wild type (WT) or N171-82Q (HD) mice treated with vehicle or LOC14 from 12 weeks of age for 6 weeks. Values are mean ± SE from three mice in each group. * $p<0.05$ compared with the WT-vehicle value; ** $p<0.05$ compared with the HD- vehicle value, two-way *ANOVA* and Bonferroni *post hoc* tests.

Figure 6. 2-((4-(cyclopropanecarbonyl)piperazin-1-yl)methyl)benzo[d]isothiazol3(2H)-one (LOC14) protected cells from mutant huntingtin by inhibiting ER stress. (**A**) Immortalized striatal cells expressing full-length wild type huntingtin (Q7) or mutant huntingtin (Q111) were exposed to serum withdrawal for 24 hrs, cells were treated with vehicle (DMSO) or LOC14 at different concentrations (5-80 nM) and ATP levels were measured at 24 h after withdrawal of serum. n= three independent experiments. *$p<0.05$ versus Q7 cells without any treatment, and *$p<0.05$ versus Q111 cells-vehicle group by two-way *ANOVA* and Bonferroni *post hoc* tests. (**B**) Representative Western blots of ER stress responsive proteins in cells with indicated treatment. Q7 or Q111 cells were treated with vehicle (DMSO) or LOC14 (40nM) for 24 h following serum withdrawal. (**C-E**) Quantification of protein levels of ER stress protein in Q7 or Q111 cells treated with vehicle or LOC14 (40 nM). Values are mean ± SE from three samples. *$p<0.05$ compared with the Q7-vehicle group; **$p<0.05$ compared with the Q111- vehicle group, two-way *ANOVA* and Bonferroni *post hoc* tests.

Abbreviations

HTT Huntingtin

HD Huntington's disease

PDI Protein disulfide isomerase

ERAD endoplasmic-reticulum-associated protein degradation

ER endoplasmic reticulum

UPR the unfolded protein response

CHOP C/EBP homologous protein

XBP1 X-box binding protein 1

Ero1 ER oxidoreductin 1

BA4 Brodmann area 4

CAG cytosine-adenine-guanine

LOC14 2-((4-(cyclopropanecarbonyl)piperazin-1-yl)methyl)benzo[d]isothiazol3(2H)-one

Wild type WT

SEM Standard error of the mean

Figure 1.

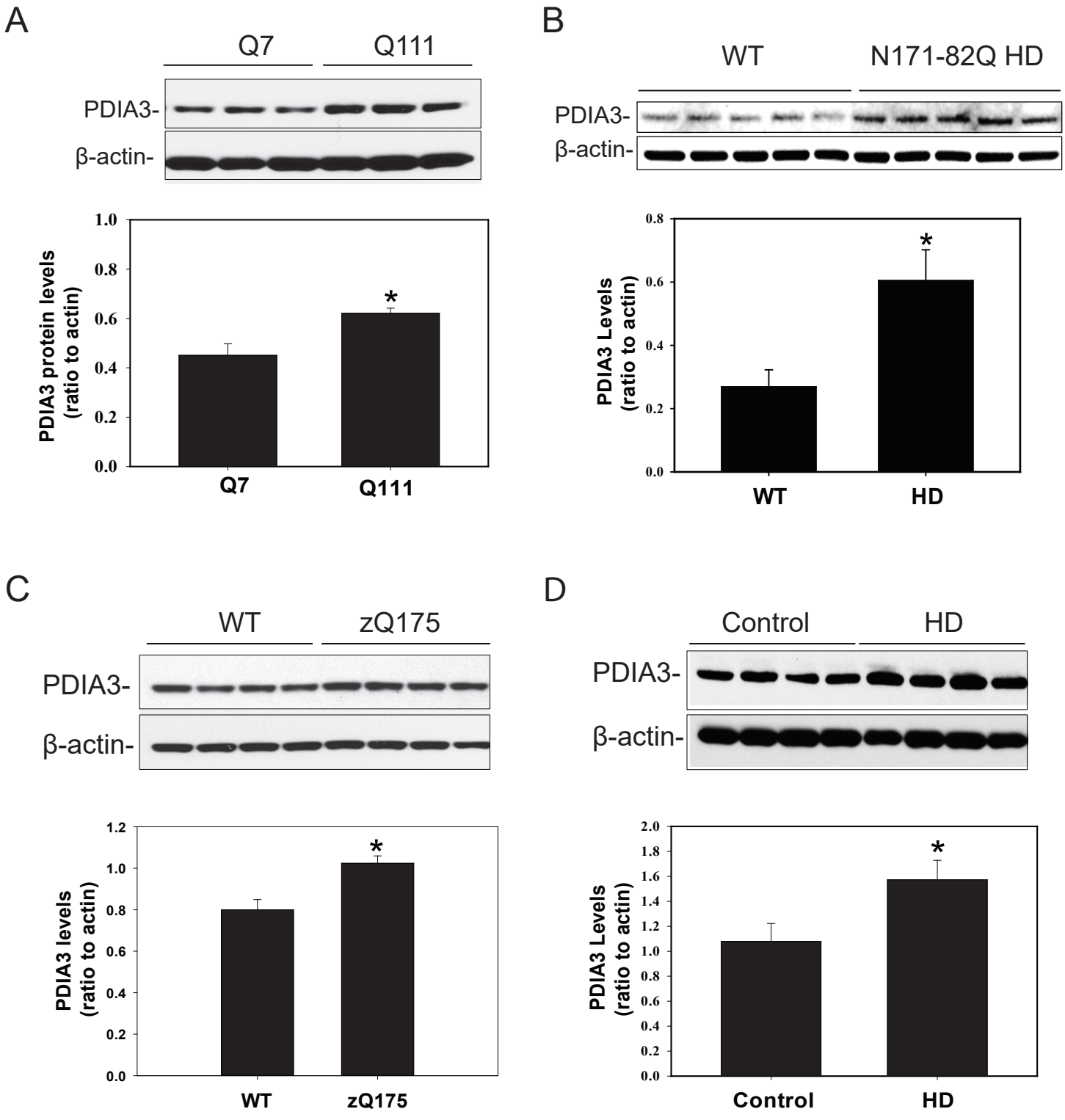

Figure 2

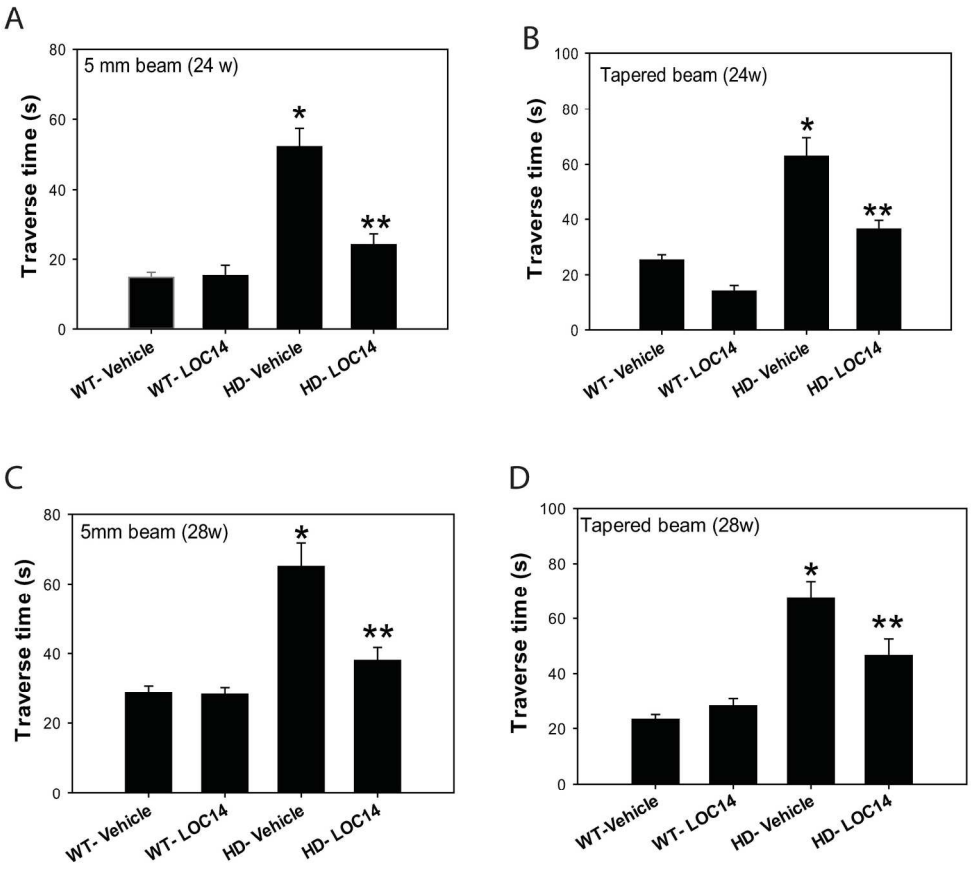

186x180mm (300 x 300 DPI)

Figure 3.

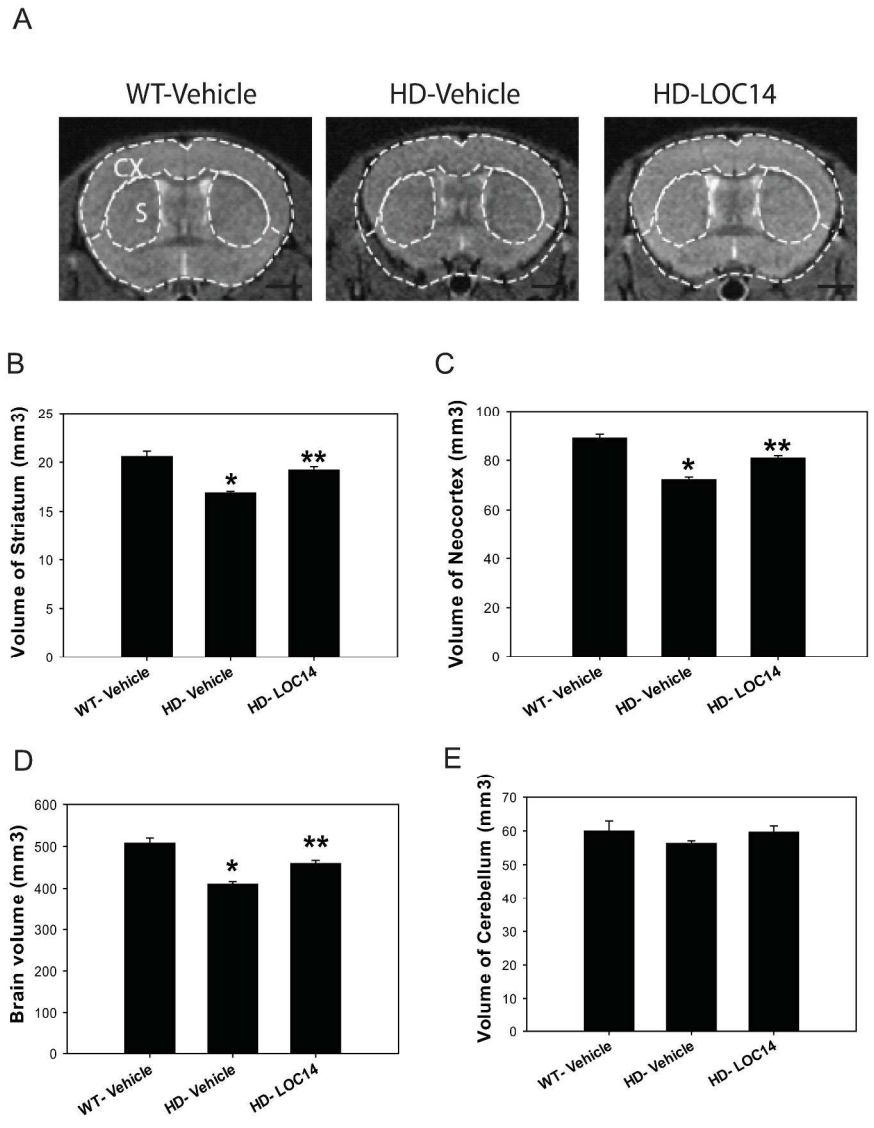

Fig 3.

266x362mm (300 x 300 DPI)

Figure 4.

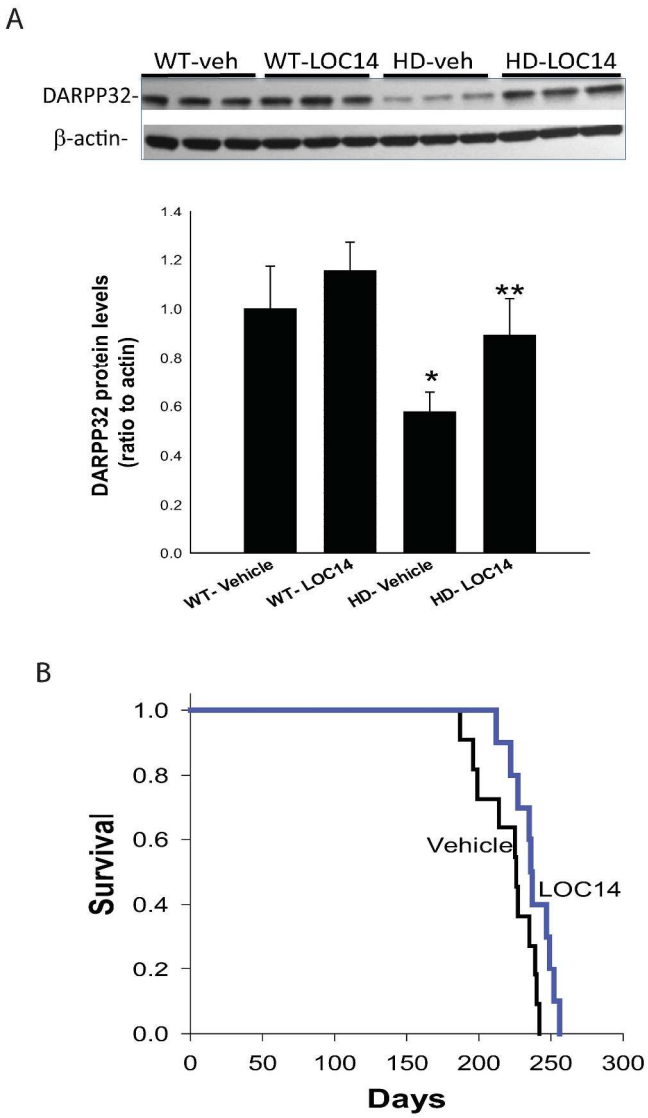

Fig 4.

250x437mm (300 x 300 DPI)

Figure 5

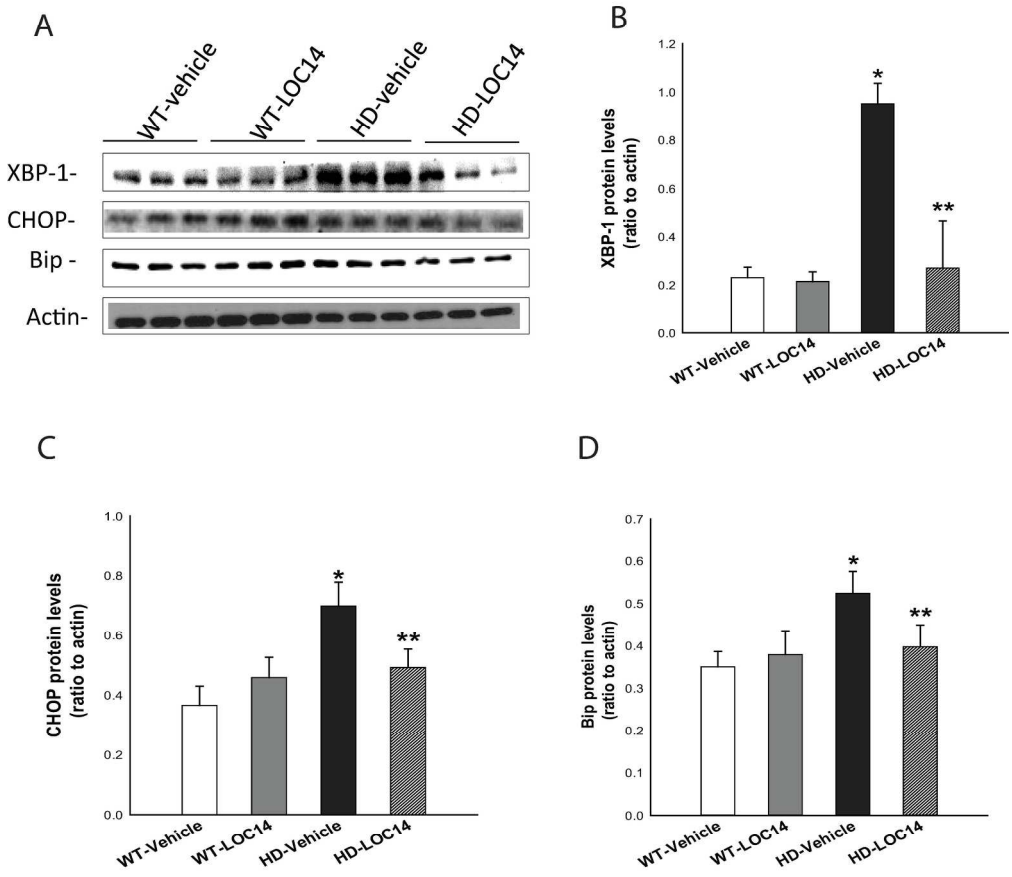

Fig 5.

212x235mm (300 x 300 DPI)

Figure 6

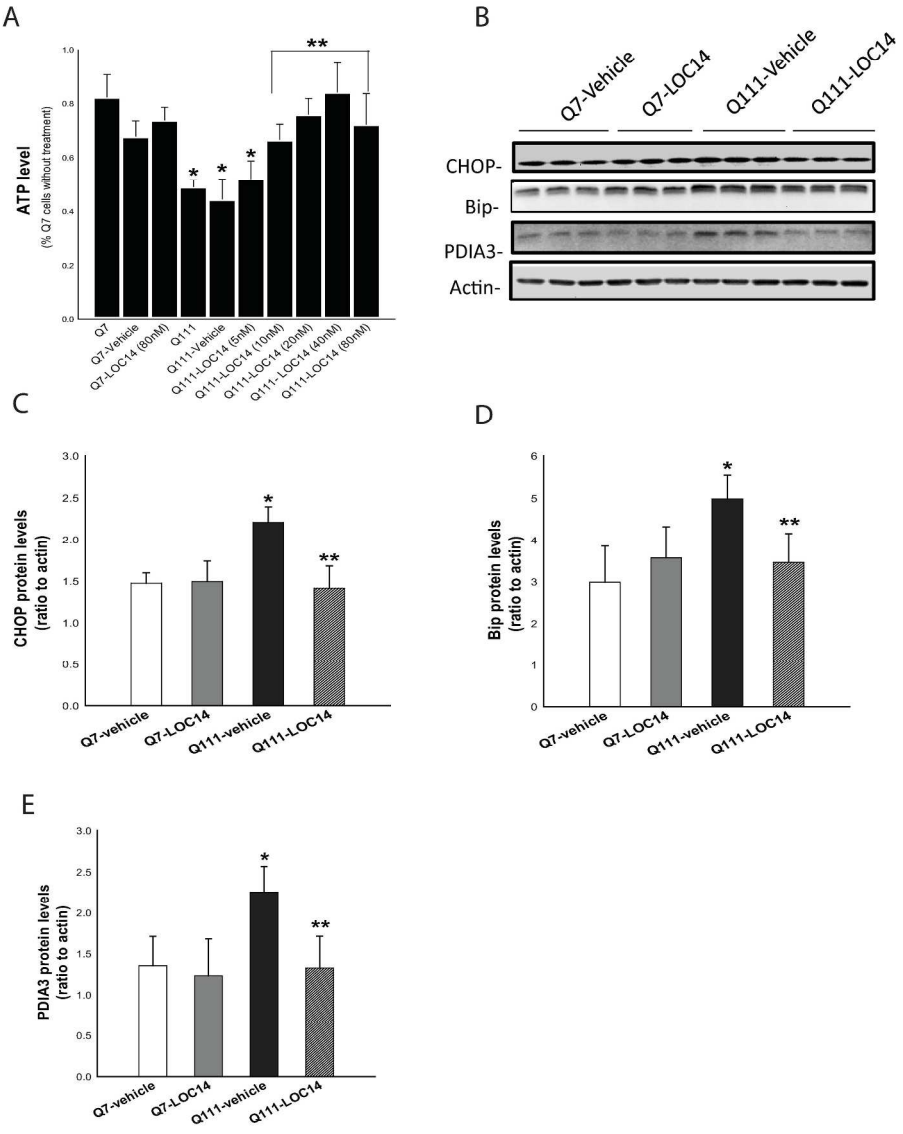

Fig 6.

264x355mm (300 x 300 DPI)